

Single-electron transistor as a radio-frequency mixer

R. Knobel, C. S. Yung, and A. N. Cleland^{a)}

Department of Physics and iQUEST, University of California, Santa Barbara, Santa Barbara, California 93106

(Received 14 March 2002; accepted for publication 10 May 2002)

We demonstrate the use of the single-electron transistor as a radio-frequency mixer, based on the nonlinear dependence of current on gate charge. This mixer can be used for high-frequency, ultrasensitive charge measurements over a broad and tunable range of frequencies. We demonstrate operation of the mixer, using a lithographically defined thin-film aluminum transistor, in both the superconducting and normal states of aluminum, over frequencies from 10 to 300 MHz. We have operated the device both as a homodyne detector and as a phase-sensitive heterodyne mixer. We demonstrate a charge sensitivity of $<4 \times 10^{-3} e/\sqrt{\text{Hz}}$, limited by room-temperature electronics. An optimized mixer has a theoretical charge sensitivity of $\leq 1.5 \times 10^{-5} e/\sqrt{\text{Hz}}$. © 2002 American Institute of Physics. [DOI: 10.1063/1.1493221]

Coulomb blockade can occur when current through a device passes through high-resistance contacts to a small-capacitance island. The condition for Coulomb blockade is that the resistance of each contact must exceed $R_K \equiv h/e^2 \approx 25.8 \text{ k}\Omega$, and the electrostatic charging energy E_C of the island must satisfy $E_C \equiv e^2/2C_\Sigma \gg k_B T$, where C_Σ is the capacitance of the island. The charging energy can be tuned electrostatically using a gate capacitively coupled to the island; the current is periodic in the gate charge, with a period e , the charge of one electron. In this mode of operation, these devices are known as single-electron transistors (SETs).^{1,2} An important application of the SET is as an ultrasensitive electrometer, with a theoretical charge sensitivity³ of order $10^{-6} e/\sqrt{\text{Hz}}$.

The high electrical resistance associated with Coulomb blockade, coupled with the unavoidable stray cable capacitance, has traditionally limited measurements with the SET to frequencies $\leq 10^4 \text{ Hz}$. This can be increased to about 1 MHz by placing a first-stage amplifier in close proximity to the SET.^{4,5} A significant innovation has recently been demonstrated,⁶ where the SET is coupled through a tuned LC tank circuit, so that at the resonance frequency $\omega_0 = 1/\sqrt{LC}$ the output impedance of the SET is matched to a 50 Ω cable. This technique, termed a radio-frequency SET (rf-SET), allows operation at resonance frequencies up to $\sim 10^9 - 10^{10} \text{ Hz}$, with a demonstrated charge sensitivity near the theoretical limit. However, the measurement bandwidth about the resonant frequency is limited to a few percent of ω_0 , as the tank circuit quality factor must satisfy $Q \geq \sqrt{2R_K}/50 \Omega \approx 30$ to achieve impedance matching. This limits applications of this device to measurements where the frequency of the signal to be measured is externally controlled, or is known beforehand to fairly high precision. In addition, the tuning circuit requires a well-characterized electrical environment, which is not always easily achieved (for example, with carbon nanotube-based transistors).

Here we demonstrate the use of the SET as a homodyne detector and as a heterodyne mixer. In the former, the non-

linear dependence of the current I on the coupled charge is employed to mix a rf signal to dc, while in the latter, the signal is mixed with a local oscillator to generate a signal at the difference frequency, close to dc, whose amplitude and phase may be measured. These techniques may be employed with any gated Coulomb blockade device, allowing measurements at frequencies up to $\omega_{\text{max}} \approx I/e$, above which nonadiabatic current transport and photon-assisted tunneling become significant.

For this experiment, we used a lithographically patterned SET, comprising two Al/AIO_x/Al tunnel junctions and two interdigitated coupling capacitors, fabricated using electron beam lithography and shadow evaporation¹ [see Fig. 1(a)]. The device was fabricated on a GaAs heterostructure to allow *in situ* fabrication of nanomechanical structures;⁷ We plan to implement the mixer as a motion sensor for a nanomechanical resonator, capacitively coupled to the SET.⁸

The device was mounted on a dilution refrigerator and cooled to $\approx 30 \text{ mK}$. All leads were filtered with metal powder filters⁹ and source and drain leads with RC filters at 1.5 K and at room temperature. The SET was operated as a mixer both in the superconducting state and in the normal state, in a magnetic field of 1 T. Figure 1(b) shows the

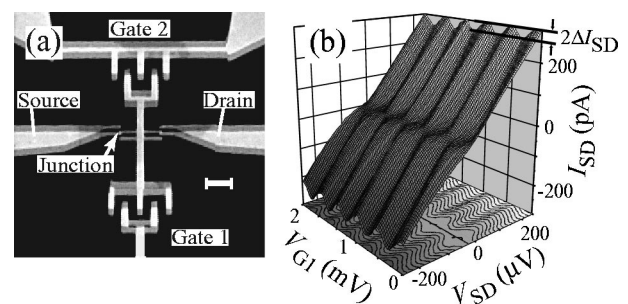


FIG. 1. (a) Electron micrograph of a typical sample, showing the $\approx 50 \times 50 \text{ nm}^2$ overlap of the junctions and the two gate capacitors. The scale bar is 1 μm . (b) dc normal-state current-voltage characteristic of the SET at 30 mK, where the modulation due to gate 1 is shown; the same behavior was seen when modulating gate 2. The device parameters extracted from this measurement are $C_{G1} = 4.2 \times 10^{-16} \text{ F}$, $C_{G2} = 2.8 \times 10^{-16} \text{ F}$, $R \equiv R_1 + R_2 = 850 \text{ k}\Omega$, and $C_\Sigma \approx 2 \times 10^{-15} \text{ F}$.

^{a)}Electronic mail: cleland@quest.ucsb.edu

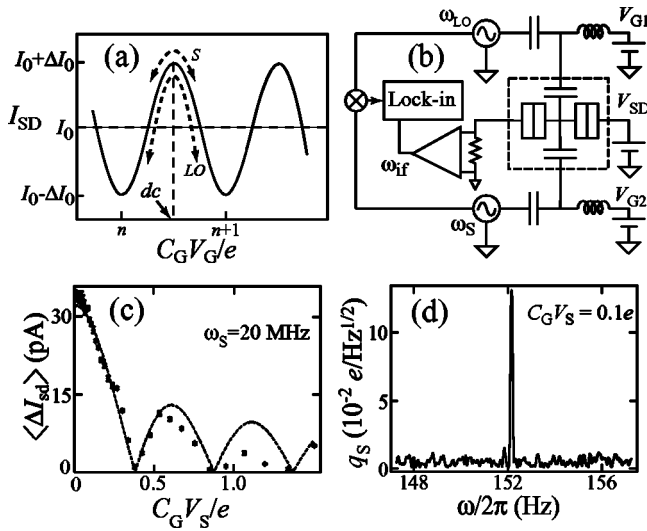


FIG. 2. (a) Schematic diagram of mixing. The gate charge is set for maximum current (dashed vertical line), and a signal and (for heterodyne mixing) local oscillator voltage are coupled to the gate. (b) Mixing circuit schematic of both homodyne and heterodyne mixing. The SET is in the dashed box in the center. (c) Homodyne detector signal at dc, measured as a function of the signal voltage. The signal at 20 MHz was applied to gate 2, while the SET was in the superconducting state. Points are experimental data, and the dashed line is the expected Bessel function response. (d) Heterodyne mixing spectral density about $\omega_{if} = 152.15$ Hz, with $C_G V_S = 0.1e$, $C_G V_{LO} = 0.3e$, $\omega_{LO}/2\pi = 20$ MHz, and $\omega_S = \omega_{LO} + \omega_{if}$, with the SET in the normal state. The vertical axis is in units of input signal charge spectral density $q_S = C_G V_S$.

normal-state current–voltage characteristic, as the dc bias on one gate was varied. The relatively large value of the SET resistance limits the noise performance and output bandwidth, as discussed below.

For near-optimal V_{SD} , as shown in Fig. 2(a), the source–drain current I_{SD} is approximately sinusoidal in the gate voltage V_G , with peak-to-peak amplitude $2\Delta I_0$ about an average value I_0 , and period e in the gate charge $C_G V_G$; at optimal source–drain bias $\Delta I_0 \approx I_0$. For homodyne detection, we bias the gate with a dc voltage V_G such that the current is at a maximum, and apply a rf voltage $V_S \cos \omega_S t$. For frequencies smaller than the tunneling rate, the dc current is then the time average of the instantaneous current $\langle I_{SD}[V_G + V_S \cos(\omega_S t)] \rangle$. At frequencies of order I/e and higher, electrons can be transferred through the SET nonadiabatically, reducing the Coulomb gap.¹⁰ At still higher frequencies, where the photon energy is comparable to the difference in final energy states $\hbar\omega \approx \Delta E$, photon-assisted tunneling can occur. This effect is negligible in our measurements.¹¹ For heterodyne mixing, we couple a local oscillator (LO) voltage $V_{LO} \cos \omega_{LO} t$ to the other gate, as shown in Fig. 2(b).

The homodyne response is shown in Fig. 2(c) for gate 2 at 20 MHz. For a model current dependence $I_{SD} \approx I_0 - \Delta I_0 \cos(2\pi C_G V_G/e)$, we expect

$$\langle I_{SD}(V_S) \rangle = I_0 + \Delta I_0 \left| J_0 \left(\frac{2\pi C_G V_S}{e} \right) \right|, \quad (1)$$

where J_0 is the zeroth-order Bessel function. A fit to this dependence is shown in Fig. 2(c); the zeroes in the response allow us to calibrate the signal voltage V_S . The nonzero

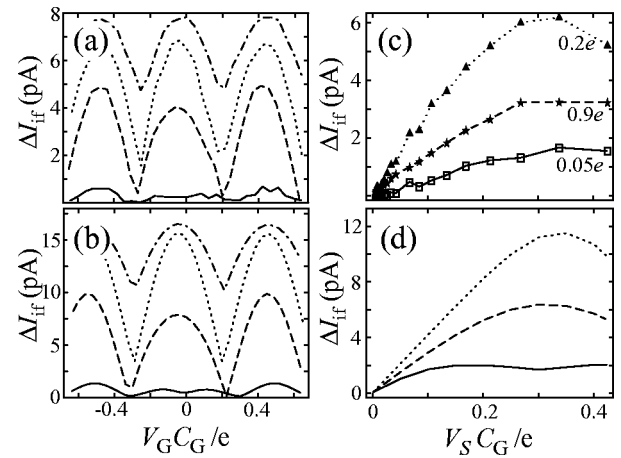


FIG. 3. (a) Amplitude of the mixing signal as a function of the dc gate charge for a range of V_{SD} (offset for clarity, with $V_{SD} = 4, 50, 100,$ and 150 μV bottom to top), with $\omega_{LO}/2\pi = 20$ MHz and $\omega_{if}/2\pi = 152.15$ Hz. (b) Modeled mixing current as a function of the dc gate charge, $V_{LO} C_G = 0.2e$, $V_S C_G = 0.25e$ at 30 mK varying V_{SD} as in (a). (c) Measured I_{if} current as a function of the rf charge on the gate for $\omega_{LO}/2\pi = 20$ MHz and $\omega_{if}/2\pi = 152.15$ Hz, with fixed source–drain bias $V_{SD} = 90$ μV . The three traces are for varying $V_{LO} C_G/e$. (d) Modeled I_{if} current for $V_{SD} = 100$ μV at 30 mK varying $V_{LO} C_G$ as in (c).

capacitance between the gate and source–drain leads can rf modulate V_{SD} as well, causing deviations from Eq. (1) at larger rf amplitudes.

For heterodyne mixing, the signal voltage is applied to one gate, and a local oscillator voltage $V_{LO} \cos \omega_{LO} t$ to the other gate. The source–drain current is modulated by both signals, and a current is generated at the intermediate frequency $\omega_{if} = |\omega_S - \omega_{LO}|$. The I_{if} signal (magnitude and phase) was detected using a lock-in amplifier, whose reference signal was generated by a separate mixer, shown in Fig. 2(b). High-pass filters ensured that this reference signal was not transmitted to the SET. The measured spectral response is shown in Fig. 2(d), showing the peak at ω_{if} as well as the sideband noise.

Figure 3(a) shows the heterodyne mixer amplitude as the dc source–drain voltage V_{SD} and dc gate voltage V_G are varied. The e periodicity in $C_G V_G$ is observed, and the dependence on V_{SD} has the expected maximum near $e/2C_S$. Figure 3(c) shows the I_{if} current as a function of signal amplitude V_S ; the same dependence is found when V_{LO} is varied. The gain of the device is tunable by varying the dc gate bias, source–drain voltage, and oscillator power. The I_{if} response was calculated using an analytic model for the SET,¹² and is shown in Figs. 3(b) and 3(d). The measured response follows the predicted behavior, but is approximately a factor of 2 smaller than calculated. At present we do not understand this discrepancy.

Figure 4(a) shows the frequency dependence of the mixer signal, for fixed ω_{if} and constant LO and signal power. Figure 4(a) shows a measurable signal up to $\omega_{LO}/2\pi \approx 300$ MHz, limited by the $\omega_{\max}/2\pi \sim 300$ MHz cut-off frequency for this device. Figure 4(b) shows the ~ 250 Hz output bandwidth for the SET. This can be increased by lowering the junction resistance, operating in the superconducting state, and reducing the cable capacitance. Use of a closely coupled preamplifier or tuned LC circuit could further increase the output bandwidth. Noise measure-

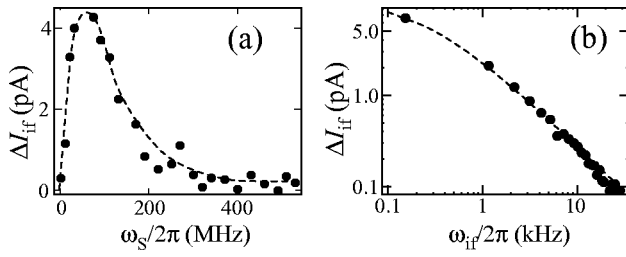


FIG. 4. (a) Mixing signal amplitude as a function of ω_{LO} at constant $\omega_{if} = 152.15$ Hz; the signal and LO powers were -68 and -61 dBm, respectively. The low-frequency rolloff is due to high-pass filtering, and the high-frequency rolloff is due to the I_{SD}/e limitation. The dashed line is a guide to the eye. (b) Mixing signal as a function of ω_{if} for $\omega_{LO} = 50$ MHz. The dashed line is a fit that gives a -3 dB single-side bandwidth of 250 Hz.

ments near the intermediate frequency ω_{if} at optimum gain yield a signal charge sensitivity $\delta q_S < 4 \times 10^{-3} e/\sqrt{\text{Hz}}$, limited by noise in the room-temperature electronics [Fig. 2(d)].

The heterodyne response can be understood by using the sinusoidal approximation for the current-charge response. The heterodyne current ΔI_{if} at ω_{if} is then related to the signal and LO voltages V_S and V_{LO} by

$$\Delta I_{if} = 2\Delta I_0 J_1\left(\frac{2\pi C_G V_S}{e}\right) J_1\left(\frac{2\pi C_G V_{LO}}{e}\right), \quad (2)$$

in terms of the first-order Bessel function J_1 . The small signal *if* current gain $g_I = \Delta I_{if}/\Delta I_S$ is optimized for V_{LO} at the first maximum of J_1 , $C_G V_{LO} \approx 0.293e$. For a current source $\Delta I_S = \omega_S C_G V_S \ll \omega_S e$, the current at optimal bias is $\Delta I_{if} = g_I \Delta I_S \approx 3.66 \Delta I_0 C_G V_S / e = 1.83(\omega_{\max}/\omega_S) \Delta I_S$. Current gain is therefore expected at frequencies below $\omega_{\max} \sim 300$ MHz for this device.

We estimate the expected charge noise for the mixer using the current shot noise $S_I(\omega) \approx 2eI_{SD}$. The output noise at ω , referenced to the input charge noise power $S_q(\omega)$, is approximately

$$S_q(\omega) = \frac{2eI_{SD}}{(\partial \Delta I_{if} / \partial q_S)^2} \approx \frac{2eI_{SD}}{(3.66 \Delta I_0 / e)^2}, \quad (3)$$

yielding input charge noise $\delta q_S(f) \approx 0.97 \sqrt{e/I_0}$. For our device this yields $\delta q_S(f) \approx 1.3 \times 10^{-4} e/\sqrt{\text{Hz}}$, while for an op-

timized SET with $R = 2R_K$, $C = 1$ fF, we find $\delta q_S(f) \approx 1.5 \times 10^{-5} e/\sqrt{\text{Hz}}$. This optimized SET would have a current gain of $g_I \approx 30$ at 100 MHz and 3 at 1 GHz. An important question remains regarding the impact of $1/f$ charge noise: If this noise modulates the mixer gain, it will contribute at ω , while if not the mixer can operate outside the $1/f$ noise-dominated band even for low ω_{if} .

In conclusion, we have demonstrated the use of a lithographically defined single-electron transistor as a radio-frequency mixer that allows the detection of signals over a fully tunable 300 MHz band. The use of this technique is complementary with SET bandwidth-enhancing techniques such as the rf-SET. The generic nature of the mixer response, and the ease with which the mixer operation can be configured, should allow its application in devices using carbon nanotubes, single molecules, and quantum dots in addition to metal tunnel junction circuits.

The authors acknowledge the financial support provided by the National Science Foundation XYZ-On-A-Chip Program, Contract No. ECS-9980734, and by the Research Corporation through a Research Innovation Award. They thank Bob Hill for processing support.

¹T. A. Fulton and G. J. Dolan, Phys. Rev. Lett. **59**, 109 (1987).

²*Single Charge Tunneling*, edited by H. Grabert and M. H. Devoret, NATO ASI Series, No. 294 (Plenum, New York, 1992).

³A. N. Korotkov, Phys. Rev. B **49**, 10381 (1994).

⁴J. Pettersson, P. Wahlgren, P. Delsing, D. B. Haviland, T. Claeson, N. Rorsman, and H. Zirath, Phys. Rev. B **53**, R13272 (1996).

⁵E. H. Visscher, J. Lindeman, S. M. Verbrugh, P. Hadley, J. E. Mooij, and W. van der Vleuten, Appl. Phys. Lett. **68**, 2014 (1996).

⁶R. J. Schoelkopf, P. Wahlgren, A. A. Kozhevnikov, P. Delsing, and D. E. Prober, Science **280**, 1238 (1998).

⁷A. N. Cleland and M. L. Roukes, Nature (London) **392**, 160 (1998).

⁸M. P. Blencowe and M. N. Wybourne, Appl. Phys. Lett. **77**, 3845 (2000).

⁹J. M. Martinis, M. H. Devoret, and J. Clarke, Phys. Rev. B **35**, 4682 (1987).

¹⁰R. J. Fitzgerald, J. M. Hergenrother, S. L. Pohlen, and M. Tinkham, Phys. Rev. B **57**, 9893 (1998).

¹¹P. K. Tien and J. P. Gordon, Phys. Rev. **129**, 647 (1963).

¹²K. Uchida, K. Matsuzawa, J. Koga, R. Ohba, S. Takagi, and A. Toriumi, Jpn. J. Appl. Phys., Part 1 **39**, 2321 (2000).